International Journal of Thermal Sciences 49 (2010) 264–271

Contents lists available at ScienceDirect

International Journal of Thermal Sciences

journal homepage: www.elsevier.com/locate/ijts

Droplet evaporation in a turbulent high-pressure freestream – A numerical study

M. Birouk*, M.M. Abou Al-Sood

Department of Mechanical and Manufacturing Engineering, University of Manitoba, Winnipeg, MB R3T 5V6, Canada

ARTICLE INFO

Article history:
Received 6 February 2009
Received in revised form
22 July 2009
Accepted 22 July 2009
Available online 14 August 2009

Keywords:
Droplet
Vaporization
Turbulence
Supercritical
Spray combustion

ABSTRACT

This paper presents a 3D numerical model for predicting the evaporation of a droplet exposed to a turbulent, high-pressure and high-temperature gaseous nitrogen freestream. The governing complete set of time-dependent conservation equations of mass, momentum, energy, and species concentration for both gas- and liquid-phase are solved numerically. The turbulence term in the conservation equations of the gas-phase is modeled by using the shear-stress transport (SST) closure model. In addition, variable thermophysical properties, unsteadiness of the gas and liquid phases, radiation, non-ideal gas behavior, and solubility of gas into the droplet are all accounted for in the numerical model. A wide range of freestream conditions is explored. The present numerical predictions revealed that the freestream turbulence intensity still has an effect on the droplet vaporization even at significantly high-pressure and high-temperature conditions, although this effect weakens with an increase in both ambient pressure and temperature. More importantly, new correlations are proposed to account for the effects of freestream ambient conditions on the droplet vaporization process.

1. Introduction

Knowledge about the vaporization process of a liquid fuel droplet is crucial for designing more efficient liquid-fueled combustion power and propulsion systems such as diesel engines, industrial burners, gas turbine jet engines, and rocket engines. Upon injection and disintegration of liquid fuel in a combustion chamber, droplets may be exposed to high-pressure, hot convective (laminar or turbulent) environments. Thus, comprehensive information about the evaporation process of an isolated droplet under such realistic conditions is of great help for developing more reliable spray combustion models.

Most of the early examinations of the vaporization process of a droplet did not include the effect of pressure. However, recent studies turned more of the attention to the role of pressure on droplet gasification and spray combustion in general. This progress was made possible thanks to the theoretical development of more reliable physical expressions capable of determining thermophysical and transport properties of fluids under high-pressure conditions. A review of recent literature revealed that there exist a considerable amount of theoretical/numerical and experimental studies on the gasification process of a droplet exposed to ambient pressure and temperature conditions similar to those encountered in a combustion chamber of liquid-fuelled combustion power systems. On the experimental front, there are only a few studies by, for example, Nomura et al. [1], Ghassemi et al. [2] and Chauveau et al. [3], which reported valuable physical evidence on the role of pressure on the vaporization of a droplet. Their findings were important not only for providing physical evidence but also for providing a bank of data for numerical validations. As for the mathematical treatment of a droplet evaporating in a high-pressure environment, several recent review and research articles studies were reported (e.g., [4–35]). However, most of these studies did not examine the coupled effect of ambient pressure and convection (laminar or turbulent flow). The exception concerns only a few studies (e.g., [4,10,26,29,34]), which investigated the effect of convective/laminar flow on the vaporization process of a liquid droplet at ambient high-pressure conditions. For instance, Meng et al. [4] and Zhang [9,10] reported useful information on the lifetime of hydrocarbon droplets evaporating in a convective environment at high-pressure in the sub-, near-, and super-critical pressure range of the liquid fuel.

The aim of the present investigation is to build upon the previous contribution of the present authors [13], as well as the contributions discussed above to develop droplet lifetime correlations similar to those developed in, e.g., [4], but over a wider range of ambient conditions not explored yet. The present examination concerns only ambient temperatures in the range above the critical temperature of *n*-heptane (the test conditions are given in Table 1). However, results over the range of ambient temperatures below the critical temperature of *n*-heptane, for the same ambient pressure and freestream turbulence intensity conditions given in Table 1, are reported in Birouk et al. [13]. It is worth nothing that over the range

* Corresponding author. Tel.: +1 204 474 8482; fax: +1 204 275 7507.
E-mail address: biroukm@cc.umanitoba.ca (M. Birouk).

1290-0729/$ – see front matter © 2009 Elsevier Masson SAS. All rights reserved.
doi:10.1016/j.ijthermalsci.2009.07.021

Nomenclature

C_p	constant-pressure specific heat
d	droplet diameter
I	turbulence intensity (u'/U_∞)
K	evaporation rate
k	turbulence kinetic energy
h	specific enthalpy
p	pressure
Re	Reynolds number
S_Φ	source term ($S_\Phi = S_C + S_P\Phi$)
T	temperature
t	time
U	mean freestream velocity
u	velocity component in x-direction
u'	RMS
v	velocity component in y-direction
w	velocity component in z-direction
Y_F	fuel mass fraction

Greek symbols

α_{eff}	effective surface absorptance
Γ	effective diffusion coefficient
Φ	diffusion parameter (u, v, w, p, T, Y_F, k, and ω)
ω	dissipation per unit turbulence kinetic energy, ε/k
σ	Steven–Boltzman constant
ρ	density
μ	viscosity

Subscript

c	critical
d	droplet
0	initial or ideal
l	liquid or laminar
r	reduced or radiation
ref	reference
s	surface
t	turbulent
v	vapor
∞	freestream

of ambient temperature $T_\infty < T_c$ [13] the droplet vaporization rate decreases (i.e. lifetime increases) with pressure, which is a completely opposite trend to that reported in the present paper.

2. Mathematical formulation of the model

The mathematical formulation of the numerical model has already been reported elsewhere (e.g., [13,36–40]). Therefore, less details are provided below.

2.1. Description of the physical model and assumptions

The physical problem consists of a liquid hydrocarbon (n-heptane) droplet, with an initial radius of r_0 and an initial uniform temperature T_0, immersed in a turbulent inert freestream of infinite expanse (nitrogen). It is assumed that the droplet remains stationary throughout its lifetime and the gas–liquid interface is at an equilibrium phase. The ambient gaseous surrounding of the droplet is prescribed by its freestream mean-velocity, U_∞, pressure, p_∞, temperature, T_∞, fuel mass fraction, $Y_{F\infty}$, turbulence intensity, I_∞, turbulence kinetic energy, k_∞, and its dissipation per unit of turbulence kinetic energy, ω_∞.

2.2. Governing equations

The governing equations for the gas-phase are the conservation of mass, momentum (i.e. Reynolds–Averaged Navier–Stokes), energy, species concentration, and turbulence kinetic energy and its dissipation rate. As for the liquid phase, the governing equations are those of mass, momentum and energy. The set of governing equations for the gas and the liquid phases can be conveniently written in a general transport equation form as follows [36]:

Table 1
Test conditions (n-heptane droplet: diameter $d_0 = 100\,\mu$m, initial temperature $T_0 = 253$ K, $T_c = 540.2$ K, $p_c = 2.74$ MPa. Freestream mean-velocity $U_\infty = 2$ m/s).

T_∞ (K)	p_∞ (MPa)	$T_r = (T_\infty/T_c)$	$p_r = (p_\infty/p_c)$	I_∞ (%) $= (u'/U_\infty)$	$Re = (\rho_\infty U_\infty d_0/\upsilon_\infty)$
594–1350	0.5–10	1.1–2.5	0.18–3.65	0–60	5–395

$$\frac{\partial}{\partial t}(\rho\Phi) + div(\rho u_i \Phi) = div\{\Gamma_\Phi grad\Phi\} + S_\Phi \quad (1)$$

where the general variable Φ may represent the mean value of mass, any of the instantaneous velocity components (u, v, w), temperature T, mass fraction of the evaporating liquid fuel Y_F, turbulence kinetic energy k or dissipation per unit of kinetic energy ω. The parameter Γ_Φ represents an effective diffusion coefficient of the general variable Φ, and S_Φ is the source term. This generalized transport equation contains four terms; transient, convection, diffusion and source. The source term includes all terms that are not explicitly accounted for in the first three terms (see Refs. [36–38]). Closure for turbulence terms in the gas-phase governing equations is obtained by using the two-equation eddy-viscosity shear-stress transport (SST) model of Menter [41]. Although the SST turbulence closure model was formulated using low pressure conditions, it has been used for solving RANS with various elevated pressure flow configurations/conditions, and it was found to produce satisfactory predictions [42,43]. Validation of RANS turbulence closure model revealed that the SST model produces the best predictions compared to all two-equation eddy-viscosity models [36,38].

Peng–Robinson Equation of State (PR-EQS) is employed to predict vapor pressure, volumetric and phase behaviors of both single and multi-component (n-heptane-nitrogen) system. This equation has been recommended for predicting vapor–liquid equilibrium at the droplet surface over a wide range of pressure conditions (e.g., [6]). Detailed information about this equation is reported in the open literature (e.g., [6,44]).

2.3. Radiation model

The radiation field inside a homogeneous liquid fuel droplet can be modeled by the radiative transfer theory (geometrical optics) [45] or the electromagnetic waves theory [46]. While, the latter neglects the radiation losses, the former is not applicable for small droplet. For large droplets, the radiation absorption by the liquid phase is limited to a thin subsurface layer [45]. An approximation of the radiation absorption that occurs only at the droplet surface with an effective surface absorptance $\propto_{\text{eff}}$ (as $\dot{q}_r = \alpha_{\text{eff}}\sigma(T_\infty^4 - T_s^4)$) is

considered in the present study; where σ is the Stefen–Boltzmann constant and the subscripts ∞ and s denote freestream and droplet surface, respectively. The value of the effective surface absorptance is based on the data of Tseng and Viskanta [45], which is a function of the droplet diameter and ambient temperature.

2.4. Gas–liquid interface conditions and vapor–liquid equilibrium at the droplet surface

The freestream mean velocity components, pressure, temperature, fuel mass fraction and turbulence quantities at the inlet of the computational domain are taken as $u = U_\infty$, $v = 0$, $w = 0$, $p = p_\infty$, $T = T_\infty$, $Y_F = 0$, $k = k_\infty$ and $\omega = \omega_\infty$. The freestream k_∞ and ω_∞ are estimated by using the following relations [41,42]: $k_\infty = 1.5(I_\infty \times U_\infty)^2$ and $\omega_\infty = \rho_\infty (k_\infty/\mu_\infty)(\mu_{t\infty}/\mu_\infty)^{-1}$, where $\mu_{t\infty}$ is the freestream turbulent viscosity which is found approximately equal to μ_∞. The conditions of the distinctive gas–liquid interface which exists at the droplet surface are obtained by coupling the conservation equations (momentum, energy and species equations) in the gas and the liquid-phases. More details are reported elsewhere [13,37,38]. The liquid and gas phases composition at the droplet surface is calculated by assuming that the system is in thermodynamic equilibrium where temperature, pressure and fugacity of each species must be equal in both phases (i.e. gas and liquid). Details are not discussed here as they are widely reported in the literature (e.g., [7,9,11,44]).

2.5. Thermophysical properties

Thermodynamic and transport properties are considered as a function of pressure, temperature and composition for the gas-phase, and as a function of only temperature and composition for the liquid-phase. For the gas phase, density is calculated by using the PR-EQS and all the other properties are expressed initially as a function of temperature and then extended to include the effect of pressure for the gas-phase. The specific heat is calculated as $c_p - c_{p,0} = (\partial/\partial T)(h - h_0)_p$ where the subscripts *0* and *p* denote ideal and constant-pressure, respectively. Thermal conductivity is calculated by using Stiel and Thodos [47] expression, viscosity is calculated by using Reichenberg [48] correlation, and diffusion coefficient is calculated by using Riazi and Whitson [49] correlation.

2.6. Numerical solution

In order to solve the complex nonlinear and strongly coupled set of governing transport equations, finite-volume approach [50] was employed. The governing differential equations are integrated over discrete volumes resulting in a set of algebraic equations having the following form

$$(a_E + a_W + a_N + a_S + a_T\Phi_T + a_B - S_P\Delta x\Delta y\Delta z)\Phi_P = a_E\Phi_E + a_W\Phi_W + a_N\Phi_N + a_S\Phi_S + a_T\Phi_T + a_B\phi_B + S_C\Delta x\Delta y\Delta z \quad (2)$$

where a_P, a_E, a_W, a_N, a_S, a_T, a_B, and b_Φ are coefficients and their expressions are reported elsewhere [36–38]. S_P and S_C are the two terms of the linearized source term S_Φ. Δx, Δy, and Δz are the dimensions of a control volume along x, y, and z coordinates, respectively. The absence of an explicit equation for pressure is dealt with by using the SIMPLEC approach [51] in which an expression in the form of Eq. (2) is derived for the pressure through a combination of the continuity and momentum equations. The end goal is to develop a pressure field such that the resulting velocity field satisfies the continuity equation for every control volume in the calculation domain. The spherical droplet in the Cartesian grid is treated by a blocking-off technique for which details of the Cartesian grid-based blocked-off treatment of a droplet immersed in the computational domain and the numerical solution are reported elsewhere (e.g., [36–40]).

The calculation domain was chosen to be a cube of $32r \times 32r \times 32r$, where r is the droplet radius [52]. The chosen optimum Cartesian grid in the calculation domain consists of $60 \times 60 \times 60$, and a very fine grid of $40 \times 40 \times 40$ is used in the domain of $4r$, i.e. $2r$ from the sphere centre in all directions. More detail is reported in previous publications of the present authors [36–40]. The solution of the set of linearized algebraic equations is accomplished by using three dimensional vectorized version of SIP (Strongly Implicit Procedure) [53].

3. Results and discussions

3.1. Vapor–liquid equilibrium (VLE) model

Preliminary calculations were carried out for vapor–liquid equilibrium (VLE) of a system that consists of *n*-heptane droplet in nitrogen environment over a wide range of ambient pressure (i.e. 0.5, 1.5, 2.7, 7, 15 and 25 MPa). These calculations revealed that the mole fraction of nitrogen dissolved into the droplet becomes significant once the ambient pressure attains the critical pressure of *n*-heptane (i.e. $p_c = 2.74$ MPa) [13]. The mole fraction of nitrogen dissolved into the droplet surface was found to increase with both ambient temperature and pressure, indicating that the single component droplet would behave as a multi-component droplet, especially, at considerably high-pressure. These calculations revealed also that the mixing critical temperature (e.g. the temperature that separates the sub-critical from the supercritical conditions of *n*-heptane droplet-nitrogen system) decreases as ambient pressure increases [13]. Consequently, the mole fraction of nitrogen dissolved into the droplet would play an important role on the mixture critical temperature.

3.2. Validation of the numerical model

The predicted turbulent vaporization rates of *n*-heptane and *n*-decane droplets were found to agree very well with their counterparts' published experimental data of Wu et al. [54] under standard pressure and temperature conditions. More details are reported elsewhere [13,38]. Also, validation of the numerical model under convective flow conditions at atmospheric pressure and high-temperature conditions were reported in [37,40]. However, published data for a droplet evaporating in a convective (turbulent or laminar) environment at high-pressure and high-temperature conditions are currently unavailable. Thus, further verification of the performance of the present numerical model is performed by comparing with published numerical and experimental data available at elevated pressure and temperature conditions in stagnant (quiescent) environment. Fig. 1 presents, for example, the temporal variation of the squared normalized diameter of *n*-heptane droplet evaporating in stagnant nitrogen at two typical ambient pressure and temperature test conditions. Fig. 1 shows that the present predictions are in good agreement with their counterparts' published experimental data. Note that validation at ambient temperatures in the range below the fuel droplet critical temperature, and ambient pressures in the range presented in Table 1, were already reported in Birouk et al. [13].

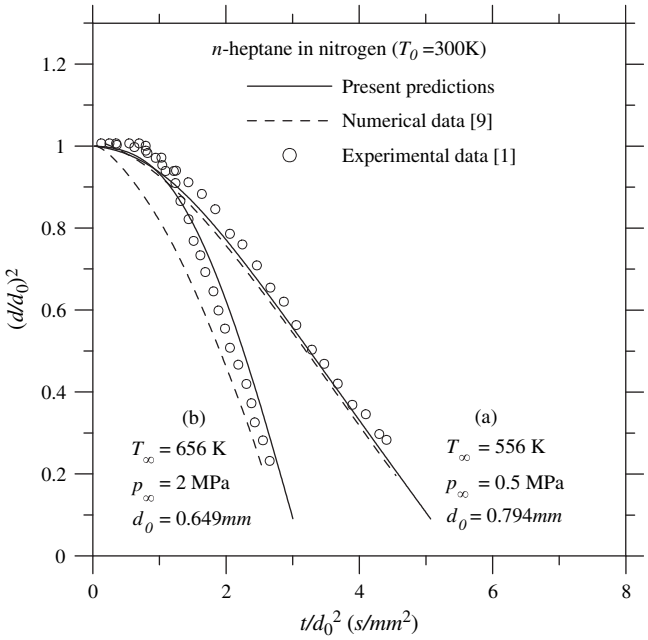

Fig. 1. Temporal variation of $(d/d_0)^2$ of *n*-heptane droplet evaporating in stagnant nitrogen (a) at $T_\infty = 556$ K and $p_\infty = 0.5$ MPa, and (b) $T_\infty = 656$ K and $p_\infty = 2$ MPa.

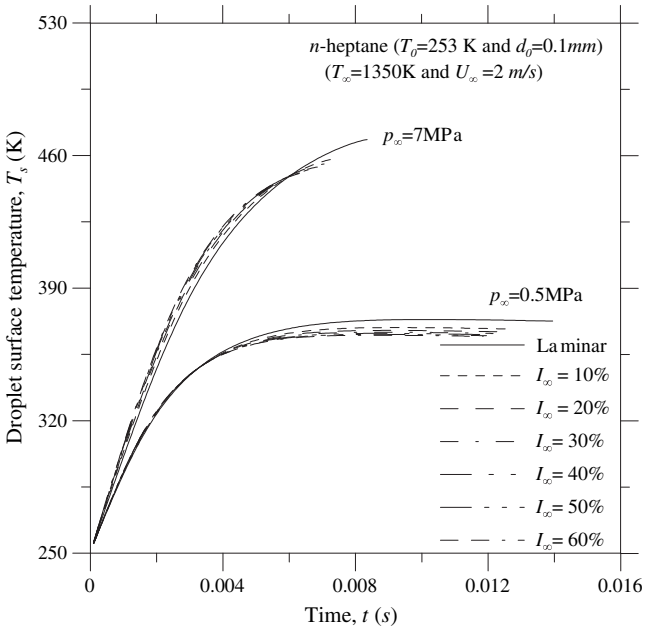

Fig. 3. Temporal surface temperature of *n*-heptane droplet for various freestream turbulence intensities.

3.3. Droplet evaporation in a turbulent convective high-pressure freestream

A parametric study is carried out to determine the variation of the droplet instantaneous vaporization rate and lifetime. The test conditions are tabulated in Table 1. Fig. 2 is a typical illustration of the temporal variation of the squared normalized droplet diameter versus freestream turbulence intensity for typical test conditions which are displayed in the figure. This figure shows that, apart from the droplet heat-up period, the vaporization process still obeys the classical d^2-law. However, the droplet evaporation process increasingly becomes transient as ambient pressure increases (not shown here but can be observed in the figures below). For example, at $p_\infty = 0.5$ MPa and $T_\infty = 1350$ K, only about 51% of the droplet lifetime obeys the d^2-law, whereas only approximately 21% at 7 MPa. More importantly, Fig. 2 reveals that the freestream turbulence intensity enhances the droplet vaporization rate (i.e., shortens the droplet lifetime) even at elevated pressure conditions. Although the effect of freestream turbulence intensity persists, it is more pronounced at low turbulence intensities, i.e. for $I_\infty < 20\%$. The relative effect of freestream turbulence intensity in relation to ambient pressure and temperature will be discussed below. Fig. 3 presents the droplet surface temperature for two-typical ambient pressures. It is clearly shown that the droplet surface temperature has two regions, i.e. transient and steady-state. For instance, the droplet surface temperature is unsteady during approximately the first half of droplet lifetime at 0.5 MPa, whereas it is unsteady almost throughout the entire droplet lifetime at 7 MPa, which is an indication of the departure from the classical d^2-law. More importantly, this figure reveals that the droplet surface temperature is higher for higher turbulence intensities during the transient period and becomes lower during the steady-state period. This suggests that turbulence enhances droplet heat transfer, as the temperature difference between the gas phase and liquid phase enlarges, which in turn enhances droplet heat and mass transfer [13].

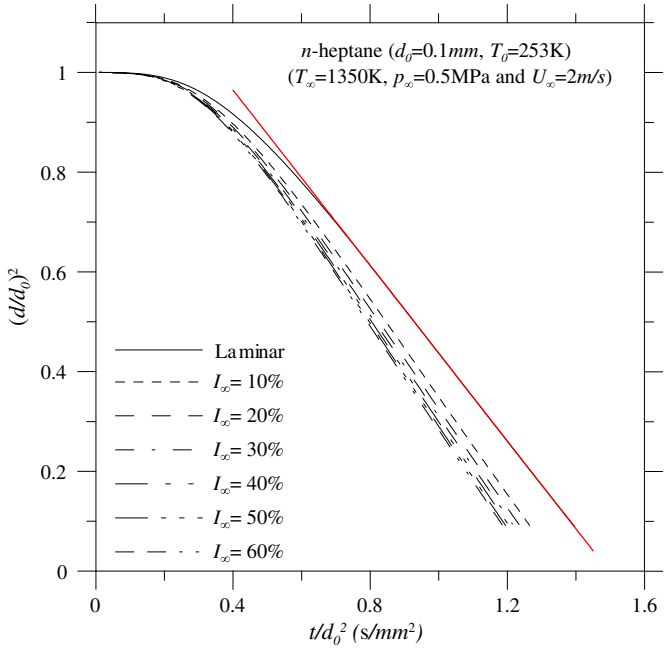

Fig. 2. Temporal variation of $(d/d_0)^2$ of *n*-heptane droplet for various freestream turbulence intensities.

Figs. 4 and 5 show the instantaneous evaporation rate of *n*-heptane droplet in nitrogen freestream for two typical ambient temperatures $T_\infty = 810$ K and 1350 K, respectively. These figures show clearly that the droplet instantaneous evaporation rate increases with both ambient temperature and pressure. Fig. 6 provides a better illustration of the relationship between the droplet average evaporation rate, ambient pressure, ambient temperature, and ambient turbulence intensity. In this figure, the droplet evaporation rate is the average value which is determined from the linear portion of the d^2 (note that this portion diminishes gradually with an increase in pressure and temperature until it vanishes completely as indicated in Figs. 4 and 5). Fig. 6 reveals that

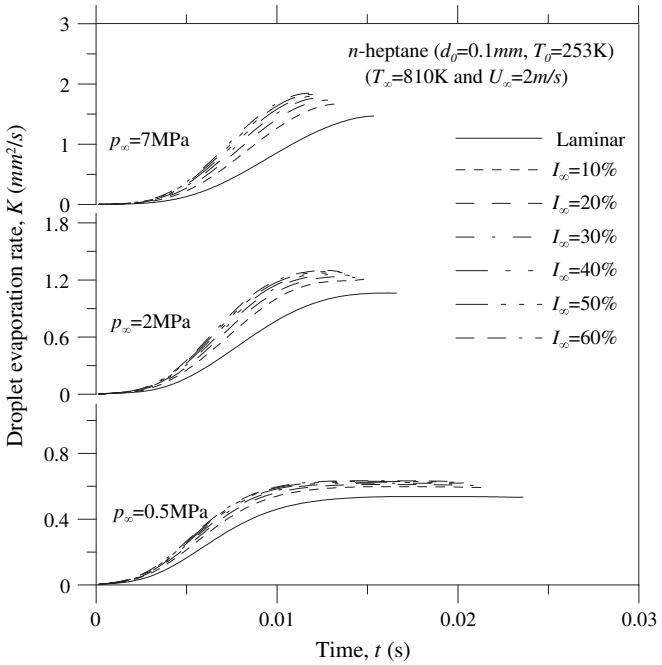

Fig. 4. Instantaneous evaporation rate of *n*-heptane droplet for various freestream turbulence intensities at a typical ambient temperature, $T_\infty = 810$ K, and various ambient pressures.

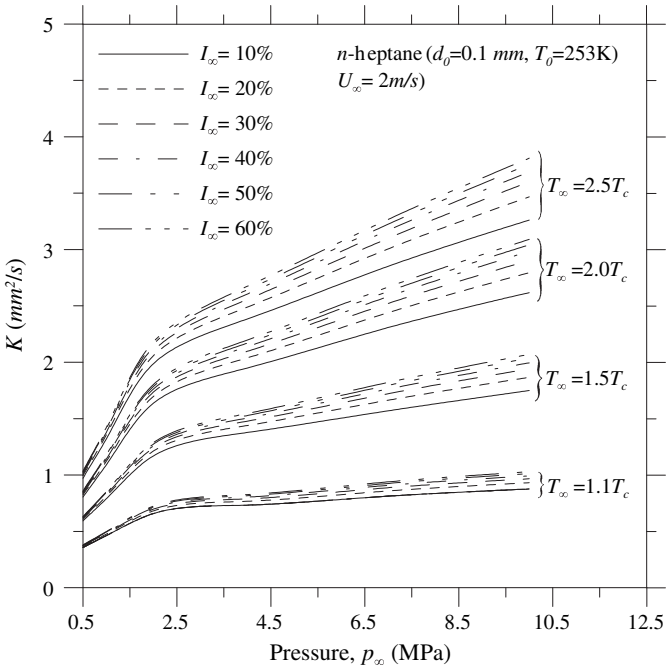

Fig. 6. Average evaporation rate of *n*-heptane droplet versus ambient pressure for various freestream turbulence intensities over a wide range of ambient temperature.

the droplet evaporation rate increases (i.e. the droplet lifetime decreases) with an increase in ambient pressure. Also, for a given ambient pressure, the droplet evaporation rate increases with turbulence intensity. Furthermore, this figure reveals that, for a given pressure and turbulence intensity, the droplet vaporization rate increases with ambient temperature. Fig. 6 interestingly exhibits two trends of the average vaporization rate while varying with ambient pressure. It shows a relatively steep linear increase up to an ambient pressure which is approximately comparable to the critical pressure of *n*-heptane, beyond which the increase in the average evaporation rate with ambient pressure slows down though it still exhibits a linear increase. Moreover, this figure reveals that the relative effect of freestream turbulence intensity on the droplet evaporation (or lifetime) weakens with ambient pressure and ambient temperature. For example, for a typical $T_\infty = 810$ K, the droplet evaporation rate increases by 10.9% at 0.5 MPa, 6.8% at 2 MPa and 5% at 7 MPa as the turbulence intensity is increased from 0% (i.e. laminar flow) to 10%. Whereas, for a typical $T_\infty = 1350$ K, the droplet evaporation rate increases by only 9.7% at 0.5 MPa, 4.7% at 2 MPa and 2.7% at 7 MPa for the same turbulence intensity increase.

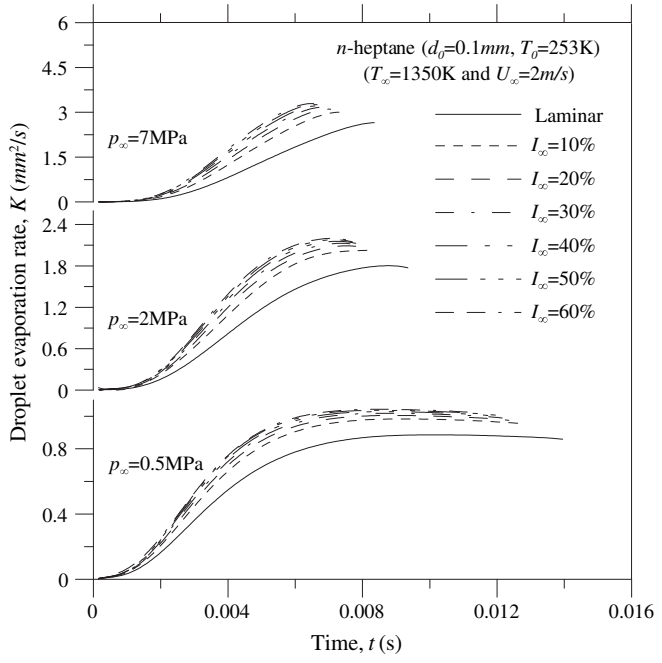

Fig. 5. Instantaneous evaporation rate of *n*-heptane droplet for various freestream turbulence intensities and at a typical ambient temperature, $T_\infty = 1350$ K, and various ambient pressures.

Since the droplet evaporation process becomes almost entirely transient at considerably high-pressure and temperature conditions, the droplet lifetime is used in order to develop useful correlations capable of describing the droplet evaporation process. Published droplet lifetime correlations under quiescent environment [10] and convective laminar flow conditions [4] are found unable to represent the present predictions. Reasons which might cause these discrepancies are tentatively discussed later on in this paper. Nonetheless, the same method used in [5] is adopted in the present study to develop a correlation of the lifetime of 100 μm in diameter of *n*-heptane droplet evaporating in a still nitrogen gaseous environment at pressure and temperature ranging between 0.5–10 MPa and 594.2–1350 K, respectively (see Table 1). The droplet lifetime, which is found to exhibit a strong dependence on the ambient pressure and temperature, is expressed as

$$\frac{t_{d,s}}{t_{d,ref}} = a\left(\frac{p - p_{ref}}{p_{ref}}\right)^b \tag{3}$$

where $t_{d,ref}$ is the droplet lifetime at a reference pressure, p_{ref} [5], which is taken in the present study to be 4.9 atm, and the coefficients a and b are constant which are found to depend strongly upon ambient temperature. It is found that these coefficients can be expressed by a third order polynomial, i.e. Eqs. (3.1)–(3.4), and are determined by employing the same procedure described in [5].

$$a = 1.466977043 - 0.976189922T_r + 0.4476927171T_r^2 - 0.0693849015T_r^3 \quad (3.1)$$

$$b = 0.1711466162 - 0.3420814236T_r + 0.1615462458T_r^2 - 0.02578594997T_r^3 \quad (3.2)$$

and

$$a = 1.056709505 - 0.0775079478T_r - 0.1533294263T_r^2 + 0.05937258384T_r^3 \quad (3.3)$$

$$b = 0.5563695741 - 1.140725269T_r + 0.6752749392T_r^2 - 0.131971775T_r^3 \quad (3.4)$$

where T_r is the reduced temperature with respect to *n*-heptane (i.e., $T_r = T_\infty/T_c$ which ranges between 1.1 and 2.5). Eqs. (3.1) and (3.2) are valid for $0.18 \le p_r \le 1.5$, and Eqs. (3.3) and (3.4) for $1.5 \le p_r \le 3.65$. This correlation, i.e. Eq. (3), which is illustrated in Fig. 7 predicts very well the droplet lifetime for the range of ambient temperature and pressure range explored in the present study.

The present data for the droplet lifetime under convective laminar freestream conditions are compared with the correlation of Meng et al. [4]. Although the present predictions have shown similar trend to the correlation of Meng et al., the discrepancy in the magnitude between the two data is quite significant. Reasons for this discrepancy are tentatively given below. The present laminar data for droplet lifetime are shown to deviate from the correlation of Meng et al. [4], as shown in Fig. 8. The best fit for the present data is found when the exponents of Reynolds number and reduced pressure are set as 0.37 and −0.27 instead of 1.26 and −1.58 as in [4], respectively. The proposed correlation, which is displayed in Fig. 9, is expressed as

$$\frac{t_{d,l}}{t_{d,s}} = \frac{1}{1 + 0.265Re^{0.37}p_r^{-0.27}} \quad (4)$$

where *Re* is the Reynolds number based on the initial droplet diameter and freestream nitrogen conditions shown in Table 1, p_r is the reduced pressure with respect to *n*-heptane (i.e. $p_c = 2.74$ MPa), and $t_{d,s}$ is the droplet lifetime in stagnant environment, which is calculated from Eq. (3). The difference between this correlation and that reported in [4] is that, in the present correlation, the droplet lifetime has weaker dependence on both the reduced pressure and Reynolds number. This difference may be caused by the way the droplet evaporates under the near-critical ambient conditions in the present study as opposed to supercritical conditions in [4]. In the present study, the hydrocarbon droplet surface temperature never attained the mixing critical state, although the maximum ambient pressure attained approximately three times the critical pressure of *n*-heptane droplet. Whereas in [4], the surface temperature of the cryogenic (liquid oxygen) droplet reached its criticality once the ambient pressure is around twice the droplet critical pressure. As the droplet surface temperature reaches the critical mixing temperature, the enthalpy of vaporization vanishes which further facilitates the droplet evaporation process [4,12]. It appears, therefore, that the vaporization process of the cryogenic droplet in [4] is considerably affected by the coupled effect of convection and surface tension which seems to be more pronounced for the cryogenic droplet over the relatively higher range of pressure conditions explored in [4] as opposed to the

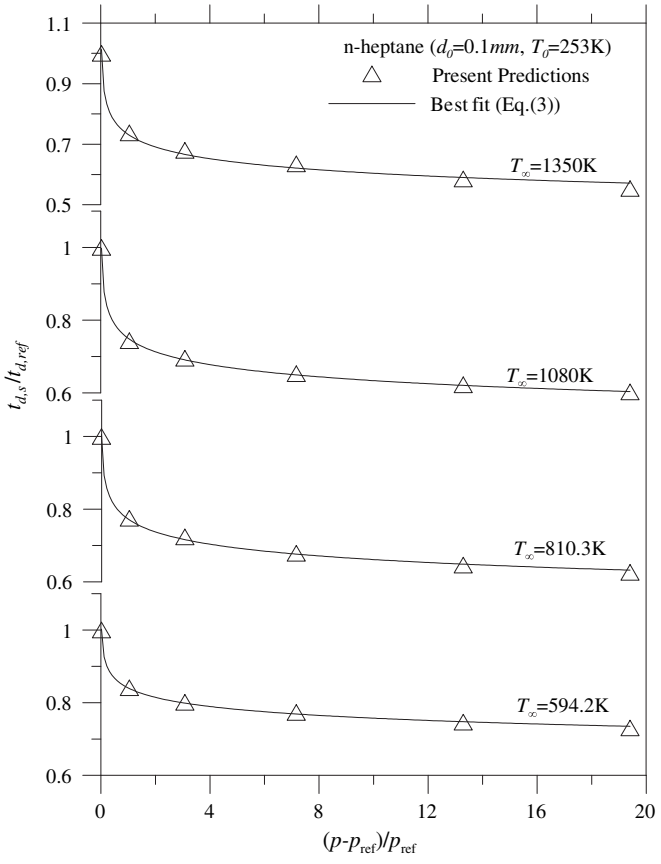

Fig. 7. Normalized droplet lifetime of *n*-heptane droplet evaporating in stagnant nitrogen over the range of p_∞ and T_∞ shown in Table 1.

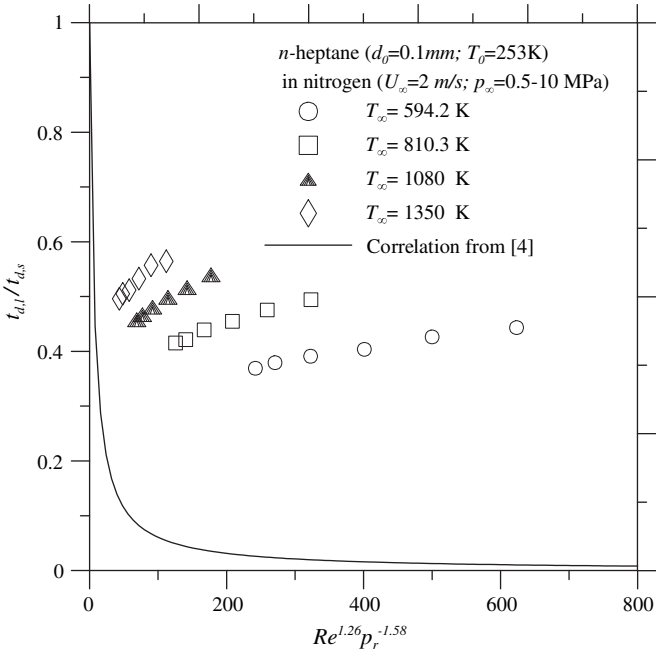

Fig. 8. Normalized droplet lifetime of *n*-heptane droplet evaporating in convective laminar nitrogen over $p_\infty = 0.5$–10 MPa, $T_\infty = 594.2$–1350 K, $U_\infty = 2$ m/s, and its comparison with the correlation of Meng et al. [3].

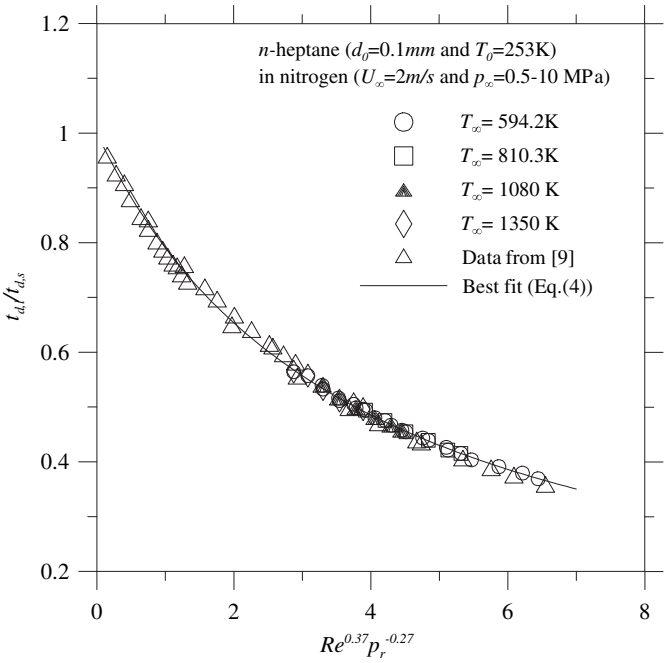

Fig. 9. Normalized lifetime of *n*-heptane droplet evaporating in convective laminar nitrogen environment over the following test conditions: $p_\infty = 0.5$–10 MPa, $T_\infty = 594.2$–1350 K and $U_\infty = 2$ m/s.

hydrocarbon droplet over the pressure range explored in the present study. This could be the reason behind the discrepancy in the order of magnitude between the present data and those reported in [4], as the data of Zhang [9], who investigated a hydrocarbon droplet over a range of ambient pressure similar to that of Table 1, collapse well onto the proposed correlation displayed in Fig. 9.

Finally, the present predictions of the droplet lifetime versus freestream turbulence intensity, for the range of ambient pressure and temperature conditions reported in Table 1, are used to develop a correlation. The best fit for the present predictions, which is plotted in Fig. 10, is found, by the help of "CurveExpert 1.3" software, to have the following expression (with coefficient of determination of 98%).

$$\frac{t_{d,t}}{t_{d,l}} = \left\{\frac{1 + 1.1964(1 + I_\infty^{0.5} T_r^{2.2} p_r^{-0.25})}{2.1447(1 + I_\infty^{0.5} T_r^{2.2} p_r^{-0.25})}\right\}^{0.957} \quad (5)$$

where $t_{d,t}$ and $t_{d,l}$ are the turbulent and laminar/convective droplet lifetimes, respectively, and I_∞ $(=u'/U_\infty)$ is the turbulence intensity. Note that, according to "CurveExpert 1.3" software, Eq. (5) should be plotted as $t_{d,t}/t_{d,l}$ versus $I_\infty^{0.5} T_r^{2.2} p_r^{-0.25}$, as shown in Fig. 10.

Eq. (5) predicts a noticeable decrease in the droplet lifetime (which in turn reflects an increase in the droplet vaporization rate) due to freestream turbulence intensity. This correlation is developed for the test conditions presented in Table 1. Interestingly this correlation shows strong dependency on reduced temperature and much less dependency upon reduced pressure and turbulence intensity.

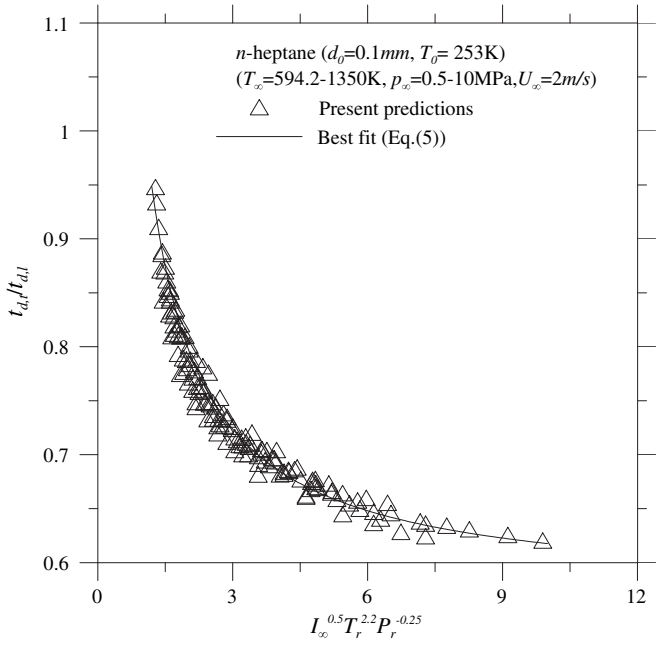

Fig. 10. Normalized lifetime of *n*-heptane droplet evaporating in turbulent nitrogen freestream over the following conditions: $p_\infty = 0.5$–10 MPa, $T_\infty = 594.2$–1350 K, $U_\infty = 2$ m/s and $I_\infty = 10$–60%.

4. Conclusion

A comprehensive 3D numerical model is developed to investigate the effect of freestream turbulence intensity on *n*-heptane droplet vaporization in the near-critical pressure and near- and super-critical temperature range of *n*-heptane droplet. The main conclusions are that the droplet lifetime decreases with both ambient pressure and temperature. More importantly, the freestream turbulence intensity enhances droplet evaporation rate (i.e. reduces droplet lifetime) but its relative effect weakens with an increase in both ambient pressure and temperature. In addition, the classical d^2-law appears to hold only for a short period of the droplet lifetime. This small period during which the d^2-law diminishes with an increase in ambient pressure and temperature until the entire droplet lifetime becomes unsteady. More importantly, correlations capable of predicting the droplet lifetime are proposed which take into considerations the effects of all ambient conditions explored here. These correlations provide useful input for spray combustion modeling under realistic conditions.

Acknowledgements

The financial support from the Natural Sciences and Engineering Research Counsel of Canada (NSERC) is gratefully appreciated.

References

[1] H. Nomura, Y. Ujiie, H.J. Rath, J. Sato, M. Kono, Experimental study of high-pressure droplet evaporation using microgravity conditions, Proc. Combust. Inst. 26 (1996) 1267–1273.
[2] H. Ghassemi, S.W. Baek, Q.S. Khan, Experimental study of evaporation of a kerosene droplet at elevated pressure and temperature, Combust. Sci. Technol. 178 (2006) 1669–1684.
[3] C. Chauveau, X. Chesneau, I. Gökalp, High pressure vaporization and burning of methanol droplets in reduced gravity, Adv. Space Res. 16 (1995) 157–160.
[4] H. Meng, G.C. Hsiao, Y. Yang, J.S. Shuen, Transport and dynamic of liquid oxygen droplet in supercritical hydrogen streams, J. Fluid Mech. 527 (2005) 115–139.
[5] V. Yang, N.N. Lin, J.S. Shuen, Vaporization of liquid oxygen (LOX) droplets in supercritical hydrogen environment, Combust. Sci. Technol. 97 (1994) 247–270.
[6] G.S. Zhu, S.K. Aggarwal, Transient supercritical droplet evaporation with emphasis on the effects of equation of state, Int. J. Heat Mass Transfer 43 (2000) 1157–1171.
[7] C. Yan, S.K. Aggarwal, A high-pressure quasi-steady droplet vaporization model for spray simulations, ASME J. Eng. Gas Turbines Power 128 (2006) 482–492.
[8] B. Abramzon, W.A. Sirginano, Droplet vaporization model for spray combustion calculations, Int. J. Heat Mass Transfer 3 (1989) 1605–1618.

[9] Zhang, H., Evaporation of a spherical moving fuel droplet over a wide range of ambient pressures within a nitrogen environment. PhD thesis, University of Nebraska, Lincoln, Nebraska, USA, 2000.
[10] H. Zhang, Evaporation of a suspended droplet in forced convective high-pressure environments, Combust. Sci. Technol. 175 (2003) 2237–2268.
[11] H. Zhang, G. Gogos, Numerical research on a vaporizing fuel droplet forced convective environment, Int. J. Multiphase Flow 30 (2004) 181–189.
[12] V. Yang, Modeling of supercritical vaporization, mixing, and combustion processes in liquid-fuelled propulsion systems, Proc. Combust. Inst. 28 (2000) 925–942.
[13] M. Birouk, M.M. Abou Al-Sood, I. Gökalp, Numerical calculation of the mass transfer rate from a single liquid fuel droplet in a low-Reynolds turbulent air flow, Combust. Sci. Technol. 11 (11) (2008) 1987–2014.
[14] S.D. Givler, J. Abraham, Supercritical droplet vaporization and combustion studies, Prog. Energy Combust. Sci. 22 (1996) 1–28.
[15] M. Arias-Zugast, P.L. Garcia-Ybarra, J.L. Castillo, Unsteady effects in droplet vaporization lifetime at subcritical and supercritical conditions, Combust. Sci. Technol. 153 (2000) 179–191.
[16] E.W. Curtis, P.V. Farrell, A numerical study of high-pressure droplet vaporization, Combust. Flame 90 (1992) 85–102.
[17] J.P. Delplanque, W.A. Sirignano, Numerical study of the transient vaporization of an oxygen droplet at su- and super-critical conditions, Int. J. Heat Mass Transfer 36 (1993) 303–314.
[18] G.H. Faeth, Evaporation and combustion of sprays, Prog. Energy Combust. Sci. 9 (1983) 1–76.
[19] P. Haldenwang, C. Nicoli, J. Daou, High pressure vaporization of LOX droplet crossing the critical conditions, Int. J. Heat Mass Transfer 39 (1996) 3453–3464.
[20] H. Hiroyasu, T. Kadota, T. Senda, T. Imamoto, Evaporation of a single droplet at elevated pressures and temperatures, Trans. JSME 40 (1974) 3147–3155.
[21] K.C. Hsieh, J.S. Shuen, V. Wang, Droplet vaporization in high-pressure environment. I: Near critical conditions, Combust. Sci. Technol. 75 (1991) 111–132.
[22] H. Jia, G. Gogos, High pressure vaporization: Effects of liquid-phase gas solubility, Int. J. Heat Mass Transfer 36 (1993) 4419–4431.
[23] T. Kadota, H. Hiroyasu, Evaporation of a single droplet at elevated pressures and temperatures, Bull. JSME 19 (1976) 1515–1521.
[24] J.A. Manrique, G.L. Borman, Calculations of steady state droplet vaporization at high ambient pressure, Int. J. Heat Mass Transfer 12 (1969) 1081–1095.
[25] R.L. Matlosz, S. Leipziger, T.P. Torda, Investigation of liquid droplet evaporation in a high temperature and high pressure environment, Int. J. Heat Mass Transfer 15 (1972) 831–852.
[26] J.P. Delplanque, W.A. Sirignano, Transcritical liquid oxygen vaporization: effects of rocket combustion instability, J. Propulsion Power 12 (2) (1996) 349–357.
[27] S.K. Aggarwal, H. Mongia, Multicomponent and high-pressure effects on droplet vaporization, ASME J. Eng. Gas Turbines Power 124 (2002) 248–257.
[28] G.S. Zhu, R.D. Reitz, S.K. Aggarwal, Gas-phase unsteadiness and its influence on droplet vaporization in sub- and super-critical environments, Int. J. Heat Mass Transfer 44 (2001) 3081–3093.
[29] J. Bellan, Supercritical (and subcritical) fluid behavior and modeling: drops, streams, shear and mixing layers, jets, and sprays, Prog. Energy Combust. Sci. 26 (2000) 329–366.
[30] J.P. Delplanque, W.A. Sirignano, Numerical study of the transient vaporization of an oxygen droplet at sub and super-critical conditions, Int. J. Heat Mass Transfer 36 (1993) 303–314.
[31] K. Harstad, J. Bellan, Isolated fluid oxygen drop behavior in fluid hydrogen at rocket chamber pressures, Int. J. Heat Mass Transfer 41 (1998) 3537–3550.
[32] Lafon, P., Modelisation et simulation numerique de l'evaporation et de la combustion de gouttes a haute pression. PhD thesis, Universite d'Orleans, France, 1995.
[33] Meng, H., Liquid-fueled droplet vaporization and cluster behavior at supercritical conditions. PhD thesis, Pen State University, USA, 2001.
[34] J.P., Delplanque, W.A. Sirignano, Transcritical vaporization and combustion of LOX droplet arrays in a convective environment, Combust. Sci. Technol. 105 (4–6) (1995) 327–344.
[35] F. Poplow, Numerical calculation of the transition from subcritical droplet evaporation to supercritical diffusion, Int. J. Heat Mass Transfer 37 (1994) 485–492.
[36] Abou Al-Sood, M.M., A numerical study of a droplet evaporating in a turbulent air flow. PhD thesis, University of Manitoba, Manitoba, Canada, 2006.
[37] M.M. Abou Al-Sood, M. Birouk, Droplet heat and mass transfer in a turbulent hot airstream, Int. J. Heat Mass Transfer 51 (2008) 1313–1324.
[38] M.M. Abou Al-Sood, M. Birouk, A numerical model for calculating the vaporization rate of a fuel droplet exposed to a convective turbulent airflow, Int. J. Num. Meth. Heat Fluid Flow 18 (2008) 146–158.
[39] M. Birouk, M.M. Abou Al-Sood, Numerical study of sphere drag coefficient in turbulent flow at low Reynolds number, Num. Heat Transfer A 51 (2007) 39–57.
[40] M.M. Abou Al-Sood, M. Birouk, A numerical study of the effect of turbulence on mass transfer from a fuel droplet evaporating in hot freestream, Int. J. Thermal Sci. 46 (2007) 779–789.
[41] F.R. Menter, Two-equation eddy-viscosity turbulence models for engineering applications, AIAA J. 32 (1994) 1598–1605.
[42] L.D. Kral, Recent experience with deferent turbulence models applied to the calculation of flow over aircraft components, Prog. Aerospace Sci. 34 (1998) 481–541.
[43] P. Lampart, Numerical optimization of a high pressure steam turbine stage, J. Comput. Appl. Mech. 5 (2004) 311–321.
[44] B.E. Poling, J.M. Prausnitz, J.B. O'connell, The properties of gases and liquids, fifth ed. McGraw-Hill, 2001.
[45] C.C. Tseng, R. Viskanta, Effect of radiation absorption on fuel droplet evaporation, Combust. Sci. Tech. 177 (2005) 1511–1542.
[46] P.L.C. Lage, R.H. Rangel, Single droplet vaporization including thermal radiation absorption, J. Thermophys. Heat Transfer 7 (1993) 502–509.
[47] L.I. Stiel, G. Thodos, The thermal conductivity of nonpolar substances in the dense gaseous and liquid regions, AIChE J. 10 (1964) 26–30.
[48] D. Reichenberg, The Viscosity of Pure Gases at High Pressures, NPL National Physical Laboratory, Teddington, England, 1975.
[49] M.R. Riazi, C.H. Whitson, Estimating diffusion coefficients of dense fluids, Ind. Eng. Chem. Res. 32 (1993) 3081–3088.
[50] S.V. Patankar, Numerical Heat Transfer and Fluid Flow, Hemisphere Publishing Corporation, 1980.
[51] J.P. Van Doormall, G.D. Raithby, Enhancement of the simple method for predicting incompressible fluid flows, Num. Heat Transfer 7 (1984) 147–163.
[52] T. Sundararajan, P.S. Ayyaswamy, Hydrodynamics and heat transfer associated with condensation on a moving drop: solution of intermediate Reynolds number, J. Fluid Mech 149 (1984) 33–58.
[53] H.J. Leister, M. Perić, Vectorized strongly implicit solving procedure for a seven-diagonal coefficient matrix, Int. J. Num. Meth. Heat Fluid Flow 4 (1994) 159–172.
[54] J.-S. Wu, Y.-J. Lin, H.-J. Sheen, Effects of ambient turbulence and fuel properties on the evaporation rate of single droplets, Int. J. Heat Mass Transfer 44 (2001) 4593–4603.